WILEY
InterScience®
DISCOVER SOMETHING GREAT

Simulated effect of a forest road on near-surface hydrologic response: redux

Benjamin B. Mirus,[1] Brian A. Ebel,[1] Keith Loague[1]* and Beverley C. Wemple[2]

[1] Department of Geological and Environmental Sciences, Stanford University, Stanford, CA 94305-2115, USA
[2] Department of Geography, University of Vermont, Burlington, VT 05405-4170, USA

*Correspondence to: K. Loague,
Department of Geological
and Environmental Sciences,
Stanford University, Stanford,
CA 94305-2115, USA.
E-mail:
keith@pangea.stanford.edu*

Abstract

In the work reported here the comprehensive physics-based Integrated Hydrology Model (InHM) was employed to conduct both three- and two-dimensional (3D and 2D) hydrologic-response simulations for the small upland catchment known as C3 (located within the H. J. Andrews Experimental Forest in Oregon). Results from the 3D simulations for the steep unchannelled C3 (i) identify subsurface stormflow as the dominant hydrologic-response mechanism and (ii) show the effect of the down-gradient forest road on both the surface and subsurface flow systems. Comparison of the 3D results with the 2D results clearly illustrates the importance of convergent subsurface flow (e.g. greater pore-water pressures in the hollow of the catchment for the 3D scenario). A simple infinite-slope model, driven by subsurface pore-water pressures generated from the 3D and 2D hydrologic-response simulations, was employed to estimate slope stability along the long-profile of the C3 hollow axis. As expected, the likelihood of slope failure is underestimated for the lower pore pressures from the 2D hydrologic-response simulation compared, in a relative sense, to the higher pore pressures from the 3D hydrologic response simulation. The effort reported herein provides a firm quantitative foundation for generalizing the effects that forest roads can have on near-surface hydrologic response and slope stability at the catchment scale. Copyright © 2006 John Wiley & Sons, Ltd.

Introduction

Dutton *et al.* (2005) employed the two-dimensional (2D) (vertical slice), transient, heterogeneous, variably saturated subsurface finite-difference flow model VS2D (Lappala *et al.*, 1993), in an event-based mode, to simulate the effect of a forest road on near-surface hydrologic response for the 1·7 ha C3 catchment (see Figure 1). The hydrologic simulations of Dutton *et al.* (2005) support the hypothesis (see Fisher, 2000; Dhakal *et al.*, 2000) that a near-surface permeability contrast, caused by the surface compaction associated with forest roads, can result in diverted subsurface flow paths that increase up-slope pore pressures, potentially initiating slope failure.

The idea that landscape evolution is governed in large part by the actions of rain and running water (Gilbert, 1880) is not new. For example, Horton (1945) noted that the development of a channel head can be controlled by erosion from baseflow contributions to streamflow (also see Dunne, 1990). Furthermore, the role of convergent topography and soil characteristics in controlling subsurface flow is an established concept in hydrology (e.g. Kirkby and Chorley, 1967; Dunne and Black, 1970a, b; Anderson and Burt, 1977, 1978). In a pioneering effort, Freeze (1971, 1972a, b) conducted three-dimensional (3D) variably saturated flow simulations (with a finite-difference model), illustrating the role of subsurface flow in streamflow generation and the rarity of Horton overland flow for steep hillslopes. A few years after Freeze, Beven (1977, 1978) conducted 2D variably saturated flow simulations (using a finite-element model), demonstrating the role of topography, slope convergence, and antecedent moisture conditions on hydrologic response.
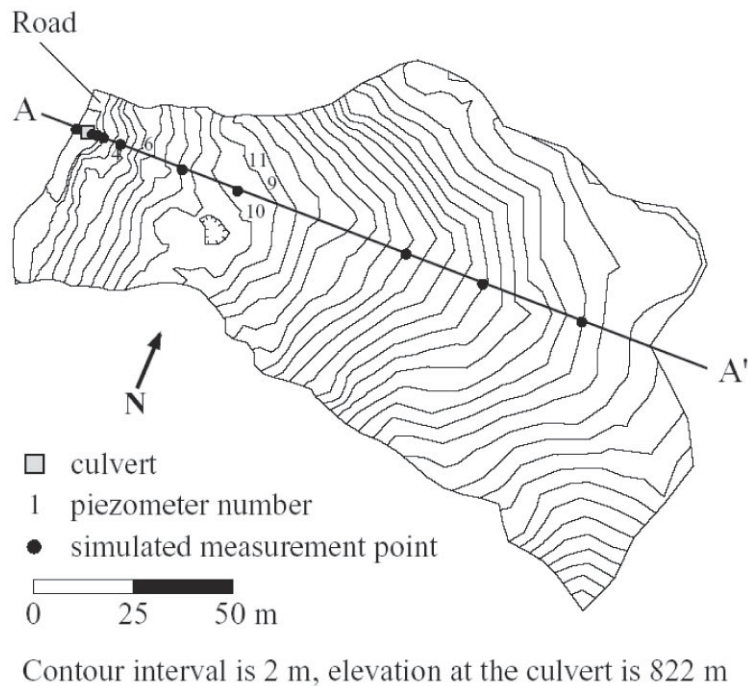
Figure 1. Topography and measurement locations for the C3 catchment (note, the location of C3 is in Figure 1 of Dutton *et al.*, 2005).

Interdisciplinary research has increasingly employed hydrologic-response simulation (albeit frequently less rigorous than the aforementioned studies by Freeze and Beven) to examine the interactions between hydrologic response (both surface and subsurface) and geomorphic processes. Hydrogeomorphology is now a recognized discipline (Sidle and Onda, 2004). Several well-known modelling efforts, focused on hydrologically driven slope stability, would now be classified as hydrogeomorphology (e.g. Hodge and Freeze, 1977; Anderson and Howes, 1985; Anderson *et al.*, 1988; Iverson and Reid, 1992; Reid and Iverson, 1992; Wu and Sidle, 1995; Wilkinson *et al.*, 2002). However, as noted by Sidle and Onda (2004): '. . . it has become increasingly apparent that many of the attempts to quantify and model hydrogeomorphic processes across various scales of time and space have been less than satisfactory due to a lack of understanding of process linkages'. It is our opinion that a critical step needed to advance the discipline of hydrogeomorphology is establishing a firm foundation based upon the rigorous characterization of surface and near-surface hydrologic processes.

The goal of the effort reported here was not to produce detailed predictions of hydrologically driven landslide initiation for the C3 forest road boundary-value problem (BVP). Instead, the primary objective of this study was to conduct and interpret a 3D simulation of near-surface hydrologic-response, using a comprehensive physics-based model, for the C3 catchment to characterize both the importance of convergent subsurface flow and the impact of a forest road. A second objective of the study was to compare the 3D C3 hydrologic-response simulation results with the results from a 2D (vertical slice) C3 hydrologic-response simulation. A third objective of this study was to conduct simple slope stability estimates for C3, driven by the 3D and 2D hydrologic-response simulations, comparing the results in a relative sense. The hydrologic-response model employed in this study was the Integrated Hydrology Model (InHM). It should be noted that the simulation effort reported herein focuses on a relatively small spatial scale (the C3 catchment) and a relatively short temporal scale (a few months), which are appropriate for investigating the nuances of a specific section of a single forest road. It is also worth pointing out that the scales of interest in this study are much smaller than for the regional-scale studies of hydrologically driven landscape evolution that have been reported in the literature during the last decade (e.g. Dietrich *et al.*, 1992, 1993, 1995; Montgomery and Dietrich, 1994; Montgomery *et al.*, 1998, 2000; Pack *et al.*, 1998). At regional (macro) scales (i.e. spatial, 10^5–10^6 m; temporal, 10^8–10^{11} s; Dooge, 1989) it is most often necessary to make simplifying assumptions related to hydrologic response that are not invoked in this study (e.g. reduced dimensionality, analytical solutions (to simplified BVPs) as operating algorithms, and/or steady-state analysis; see Loague *et al.*, 2006).

Table I. Summary of the ten largest storms recorded at H. J. Andrews Experimental Forest based upon hourly data from 1 December 1985 to 30 September 1998. The storms are ranked in order of decreasing cumulative depth

Date*	Depth (mm)	Mean intensity (mm h^{-1})	Duration (days)	Peak intensity (mm h^{-1})	Time since last storm (days)
4 Dec. 1996†	356	1·5	9·8	10·9	0·9
22 Dec. 1996†‡	289	2·1	5·7	10·9	0·2
5 Feb. 1996	250	4·9	2·1	10·9	0·1
15 Nov. 1996†	249	1·5	6·9	7·1	0·1
9 Jan. 1998	204	1·3	6·4	7·9	1·4
30 Jan. 1997	151	2·0	3·1	8·4	1·5
3 Jan. 1994	147	0·6	9·7	1·6	0·1
26 Apr. 1990	134	4·5	1·3	9·1	0·7
27 Nov. 1996†§	129	1·1	5·0	6·4	1·8
9 Jan. 1988	129	3·1	1·8	6·1	0·1

* Start of storm.
† Storms simulated in this study.
§ Event number 2 in Dutton *et al.* (2005).
‡ Event number 3 in Dutton *et al.* (2005).

Table II. Characteristics of the C3 boundary-value problem

Layer*	Unit	Depth (m)	Porosity (–)	Saturated hydraulic conductivity (m s^{-1})	Compressibility (m s^2 kg^{-1})
I	Road	1·0†	0·4†	1×10^{-8}†	1×10^{-9}‡
II	Soil (layer 1)	1·5†	0·4†§	1×10^{-3}†§	1×10^{-7}‡
III	Soil (layer 2)	1·5†	0·4†‖	7×10^{-4}†‖	1×10^{-7}‡
IV	Bedrock	100	0·2‡	1×10^{-9}‡	1×10^{-9}‡

* See Figure 2.
† Dutton (2000).
‡ Freeze and Cherry (1979).
§ Averaged from 36 measurements (Dutton, 2000).
‖ Averaged from 12 measurements (Dutton, 2000).

C3 Catchment

The C3 catchment is located in the WS3 watershed within the H. J. Andrews Experimental Forest (Dutton *et al.*, 2005). Established in 1932, the H. J. Andrews Experimental Forest (HJAEF) has been host to considerable research focused on the effects of forest management practices (see http://www.fsl.orst.edu/lter/). The impact of forest roads has been well documented for the HJAEF (e.g. Swanson and Dyrness, 1975; Jones and Grant, 1996; Thomas and Megahan, 1998; Wemple *et al.*, 2001; Wemple and Jones, 2003; Dutton *et al.*, 2005). Previous hydrologic-response simulation efforts at the HJAEF include the works by Tague and Band (2001), Wemple and Jones (2003), Kokkonen *et al.* (2004), and Waichler *et al.* (2005).

The C3 site was selected by Dutton *et al.* (2005), and subsequently the effort reported herein, because of its concave topography, sparse understorey vegetation, prior field investigation (see Wemple and Jones, 2003), and, importantly, a dissecting road. The road and convergent C3 topography are shown in Figure 1. The average long-profile (see A–A′ in Figure 1) slope of the catchment is 18·3° (32 per cent). The location of the C3 culvert (at the road) is shown in Figure 1. The ten largest storms recorded for the HJAEF, for the period 1985–1998, are summarized in Table I.

A cross-section of the C3 BVP, showing the four hydrogeologic units (see Table II), is given in Figure 2. Due to limited information with which to characterize the subsurface units, each layer was taken to be of uniform thickness. Although not a perfect representation of the C3 subsurface, the uniform layers do capture the measured soil depths within the hollow of the catchment (Dutton, 2000). The uniform layers also facilitate a more direct comparison between the 3D and 2D simulations reported herein. At each of the ten simulated measurement locations (see Figure 2) subsurface pore pressures are reported at 0·5 m below the surface and at a depth of 3 m (i.e. the soil/bedrock contact).
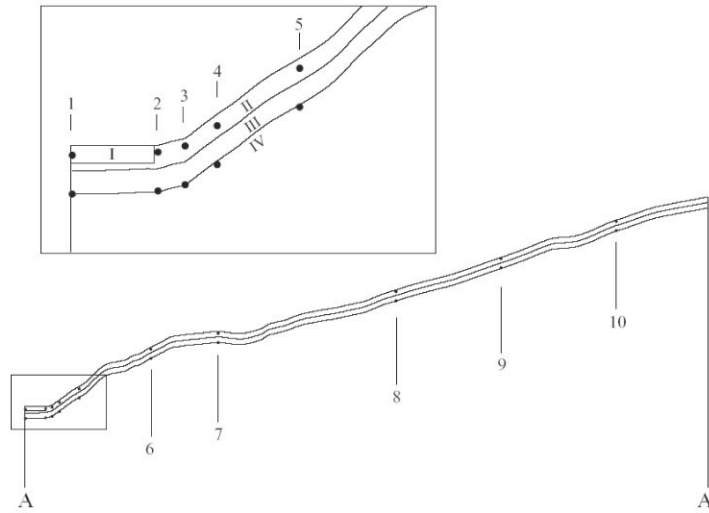
Figure 2. Cross-section showing the four idealized hydrogeologic units and simulated measurement locations for the C3 catchment (see Table II for characterization of the individual units).

Integrated Hydrology Model (InHM)

In the spirit of the Freeze and Harlan (1969) blueprint, the comprehensive InHM was designed to quantitatively simulate, in a fully coupled approach, 3D variably saturated flow and solute transport in porous media and macropores and 2D flow and solute transport over the ground surface and in open channels. The fundamental and innovative characteristics of InHM, including no *a priori* assumption for a specific hydrologic-response mechanism (i.e. Horton or Dunne overland flow, discharge from subsurface stormflow or groundwater; see Freeze, 1980), are discussed elsewhere (VanderKwaak, 1999; VanderKwaak and Loague, 2001; Loague and VanderKwaak, 2002, 2004; Loague *et al.*, 2005). InHM has been successfully employed for catchment-scale, event-based rainfall–runoff simulation (VanderKwaak and Loague, 2001; Loague and VanderKwaak, 2002; Loague *et al.*, 2005) and for solute transport simulations (VanderKwaak, 1999; Jones *et al.*, 2004). Recently, Heppner *et al.* (2006) added and tested a sediment transport algorithm to InHM. The macropore, solute transport and sediment transport components of InHM are not employed for the effort reported herein.

InHM estimates subsurface flow by:

$$\nabla \cdot f^a \vec{q} \pm q^b \pm q^e = f^v \frac{\partial \phi S_w}{\partial t} \tag{1}$$

where f^a is the area fraction associated with each continuum [–], $\vec{q}$ is the Darcy flux [L T^{-1}], q^b is a specified rate source/sink [T^{-1}], q^e is the rate of water exchange between the subsurface and surface continua [T^{-1}], f^v is the volume fraction associated with each continuum [–], ϕ is porosity [–], S_w is water saturation [–], and t is time (T). The Darcy flux is given by:

$$\vec{q} = -k_{rw} \frac{\rho_w g}{\mu_w} \vec{k} \nabla(\psi + z) \tag{2}$$

where k_{rw} is the relative permeability [–], ρ_w is the density of water [M L^{-3}], g is the gravitational acceleration [L T^{-2}], μ_w is the dynamic viscosity of water [M L^{-1} T^{-1}], $\vec{k}$ is the intrinsic permeability vector [L^2], z is the elevation head [L], and ψ is the pressure head [L]. The relationship between pressure head and pore water pressure [ML^{-1} T^{-2}] is given by:

$$p = \rho_w g \psi \tag{3}$$

InHM estimates the transient flow of water on the land surface by the diffusion wave approximation of the depth-integrated shallow water equations. Such 2D surface flow is conceptualized as a second continuum that interacts with

the underlying variably saturated porous medium through a thin soil layer of thickness a_s [L]. Assuming a negligible influence of inertial forces and a shallow depth of water, ψ_s [L], the conservation of water on the land surface is described by:

$$\nabla \cdot \psi_s^{mobile} \vec{q}_s \pm a_s q^b \pm a_s q^e = \frac{\partial (S_{w_s} h_s + \psi_s^{store})}{\partial t} \tag{4}$$

where $\vec{q}_s$ is the surface water velocity [L T^{-1}], q^b is the source/sink rate (i.e. rainfall/evaporation) [T^{-1}], q^e is the surface–subsurface water exchange rate [T^{-1}], and h_s is the average height of non-discretized surface microtopography [L]; the superscripts *mobile* and *store* refer to water exceeding and held in depression storage, respectively (VanderKwaak, 1999). Surface water velocities are calculated utilizing a two-dimensional form of the Manning's equation given by:

$$\vec{q}_s = -\frac{(\psi_s^{mobile})^{2/3}}{\vec{n}\Phi^{1/2}} \nabla(\psi_s + z) \tag{5}$$

where $\vec{n}$ is the Manning's surface roughness tensor [T L$^{-1/3}$] and Φ is the friction (or energy) slope [–]. The linkages between Equations 1 and 4 are through first-order, physically based flux relationships driven by pressure head gradients.

The subsurface and surface flow equations are discretized in space using the control volume finite-element method. Each coupled system of non-linear equations is solved implicitly using Newton iteration (VanderKwaak, 1999). Efficient and robust iterative sparse matrix methods are used to solve the large sparse Jacobian systems (VanderKwaak, 1999).

Methods

Boundary-value problem

Figure 3 shows the finite-element mesh used to represent the C3 catchment for the InHM simulations in this study. The C3 mesh consists of 145 460 prism elements for the subsurface (80 088 InHM equations) and 2078 triangular elements for the surface (1128 InHM equations). The vertical nodal spacing (Δz) in the C3 mesh varies from 0·02 m (near surface) to 13 m (at depth); the horizontal nodal spacing (Δx, Δy) varies from 0·7 m (hollow axis) to 20 m
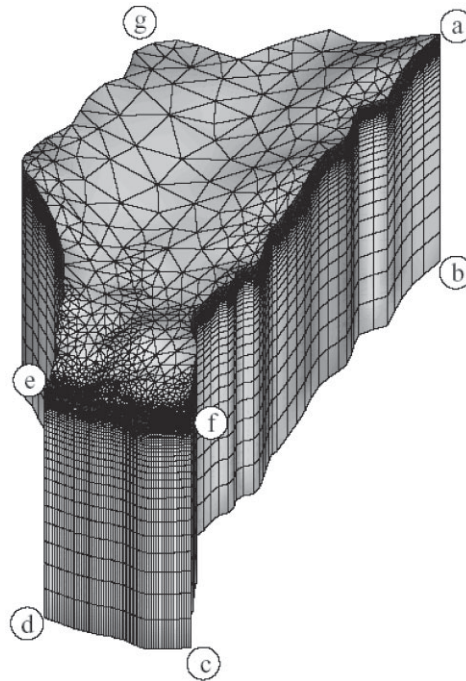

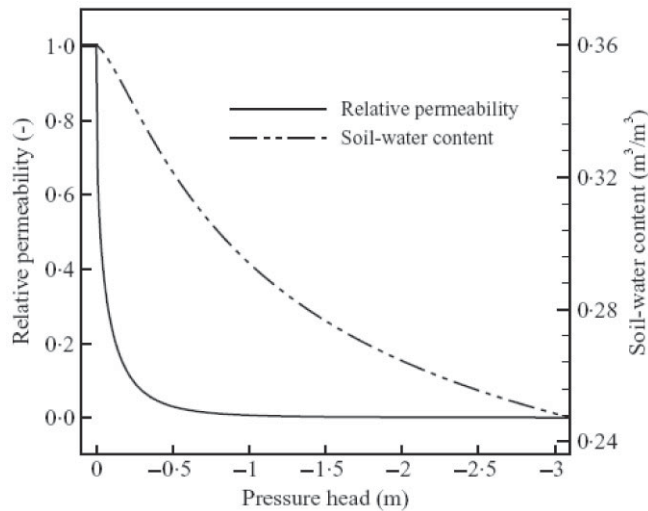**Figure 3.** Three-dimensional finite-element mesh used to represent the C3 catchment.

Figure 4. Characteristic curves used to represent the near surface of the C3 catchment.

(edges). An adaptive time step (Δt) was used for the InHM simulations in this study. With reference to the lettered coordinate locations identified in Figure 3, the subsurface boundary conditions for each face of the C3 BVP are as follows: impermeable (f–a–b–c, g–a–b–h, e–g–h–d, d–c–b–h), local sink (e–f–c–d), and flux (e–g–a–f). The local sink value (i.e. a point of constant head), based upon the average value from a piezometer 15 m down-gradient of the road, is 815·7 m (Wemple, 1998). The surface boundary conditions (see Figure 3) are impermeable (e–g–a–f) except at the culvert, where there is a critical depth of 0 m. With reference to the lettered coordinates in Figure 3, the dimensions of the C3 BVP are as follows: *c.* 103 m for e–d/f–c/a–b/g–h, *c.* 73 m for e–f/d–c, *c.* 119 m for g–a/h–b, *c.* 187 m for e–g/d–h, and *c.* 215 m for a–f/b–c.

Parameterization of the C3 BVP units for the InHM simulations in this study is summarized, in part, in Table II. The soil-water retention and permeability functions, based upon experimental data from Dutton (2000) and the approach of van Genuchten (1980), are shown in Figure 4. The mobile water depth (i.e. depression storage) and the height of micro-topography were both set at 0·002 m. The Manning's roughness coefficient was taken as 0·3 (Engman, 1985). The values for g, ρ, and μ in Equation 2 were taken (Freeze and Cherry, 1979) as 9·8 $m^2\ s^{-1}$, 1000 $kg\ m^{-3}$, and 0·001138 $kg\ m^{-1}\ s^{-1}$, respectively.

An estimate of the initial 3D pressure-head distribution is needed for transient simulations of unsaturated–saturated flow with InHM. Draining the catchment (via simulation) to determine initial conditions provides a physics-based and internally valid estimate of the continuous head field (VanderKwaak and Loague, 2001). The only calibration component to the simulations reported here was draining the catchment for the acquisition of initial conditions. Two steps were employed to obtain initial conditions: (i) the catchment was drained from a nearly saturated state until the simulated discharge was approximately zero, and then (ii) a 48-day warm-up period (prior to time A in Figure 5) was simulated using observed rainfall. At the start of the observed discharge (time A in Figure 5), the matches between the observed and simulated discharges were acceptable. It is worth noting that the records (Wemple, 1998) from five piezometers (see Figure 1) were used to qualitatively judge the acceptability of the initial conditions for the C3 simulations in this study. It was, however, not possible for this study to quantitatively compare the total heads from the piezometers and the simulations as the dimensions associated with the measurements (e.g. screened interval) were unknown, relative to the assumed uniform layers and the resolution of the surface topography (i.e. 3 m DEM), with sufficient accuracy (<1 m).

The parameterization of the C3 BVP for the effort reported here honours all of the reliable information/data that were available for the catchment. It is worth noting that more detailed InHM simulations would have been possible for C3 if supplemental information/data had been available (e.g. detailed characterization of the hydrogeologic layer geometry).

Continuous simulation

The InHM simulation of hydrologic response was continuous in this study. Figure 5 shows the rainfall hyetograph used to drive the InHM simulation of hydrologic response for C3. The hourly rainfall record in Figure 5 is 91 days in
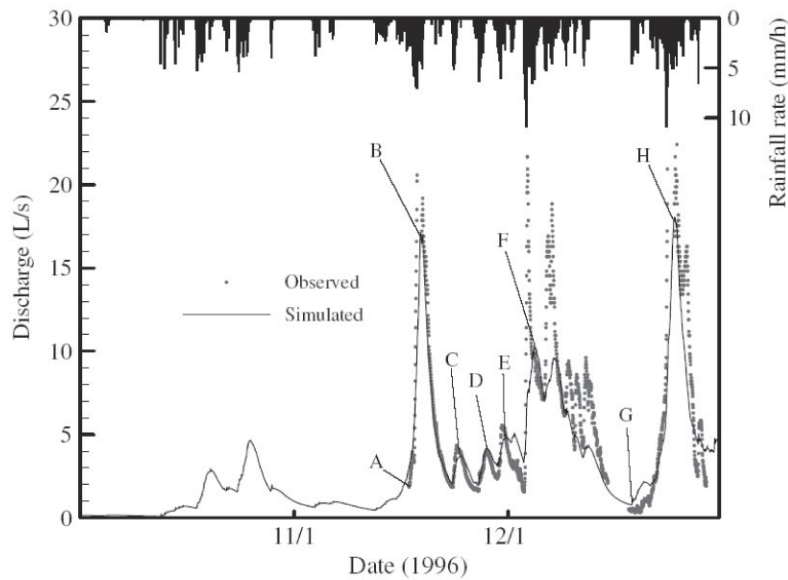
Figure 5. Observed versus InHM simulated C3 discharges for a November – December 1996 period that includes six runoff events. The InHM warm-up period ends (runoff event 1 starts) at time A. Times B, C, D, E, F and H are at the simulated peak discharge for runoff events 1 to 6, respectively. Time G is at the end of the break in rainfall between runoff events 5 and 6. The location of the culvert is shown in Figure 1.

length (1 October to 30 December 1996), containing six observed runoff events. The six runoff events in this study are driven by four of the ten storms summarized in Table I (note, runoff events 2, 3 and 4 result from a storm that began on November 27 1996; see Table I). After the warm-up period, used to estimate initial conditions, simulated discharges (at the culvert) were compared to the observed discharges (see Figure 5). Despite the ability of InHM to consider evapotranspiration, neither evaporation from the soil profile nor transpiration from the overstorey (primarily Douglas fir, *Pseudotsuga menziesii*) were considered in this study for C3, due to the uncertainty in the meteorological record (i.e. proximity to the catchment) and the prolonged nature (see Figure 5) of the storms (i.e. the arguably near-saturated relative humidity within the surface boundary layer).

Model performance evaluation

The measure of model performance used to test InHM is modelling efficiency (*EF*). The expression for *EF* is (James and Burges, 1982; Loague and Green, 1991; Pebesma *et al.*, 2005):

$$EF = \left[\sum_{i=1}^{n} (O_i - \bar{O})^2 - \sum_{i=1}^{n} (P_i - O_i)^2 \right] / \sum_{i=1}^{n} (O_i - \bar{O})^2 \tag{6}$$

where P_i are the predicted values, O_i are the observed values, n is the number of samples, and $\bar{O}$ is the mean of the observed data. When the observed and simulated values are identical the *EF* statistic is 1·0.

Results

The results from the InHM simulations of C3 are summarized in Table III and Figures 5–9. Table III lists the InHM model performance statistics for the entire simulation period and the six individual runoff events. Table III also compares the observed peak discharge and time to peak discharge with the corresponding InHM simulated values for the six individual runoff events. Figure 5 shows the observed and simulated hydrographs (notes: time A identifies the start of the observed/simulated comparison; times B, C, D, E, F and H identify the simulated peak discharges for runoff events 1 to 6, respectively; time G identifies the start of runoff event 6 after a five-day break in rainfall).

Table III. Model performance, peak, and time to peak for observed versus InHM simulated discharges at the C3 culvert (see Figure 1 for culvert location)

Runoff event†	EF‡	Peak discharge (l s⁻¹)			Time to peak discharge (days)*		
		Observed	Simulated	Percentage difference	Observed	Simulated	Percentage difference
1–6§	0·75	–	–	–	–	–	–
1	0·84	20·6	17·1	17	1·2	1·7	39
2	0·73	4·3	3·7	14	0·5	1·2	124
3	0·38	4·1	4·2	1	1·2	1·1	2
4	−0·29	5·5	5·0	9	0·6	1·2	93
5	0·49	21·7	10·6	51	0·4	1·5	238
6	0·79	22·4	18·0	20	7·0	6·6	5

* Time to peak (observed/simulated) minus the start time for the observed runoff event.
† See Figure 5 for identification of individual runoff events
‡ Modelling efficiency.
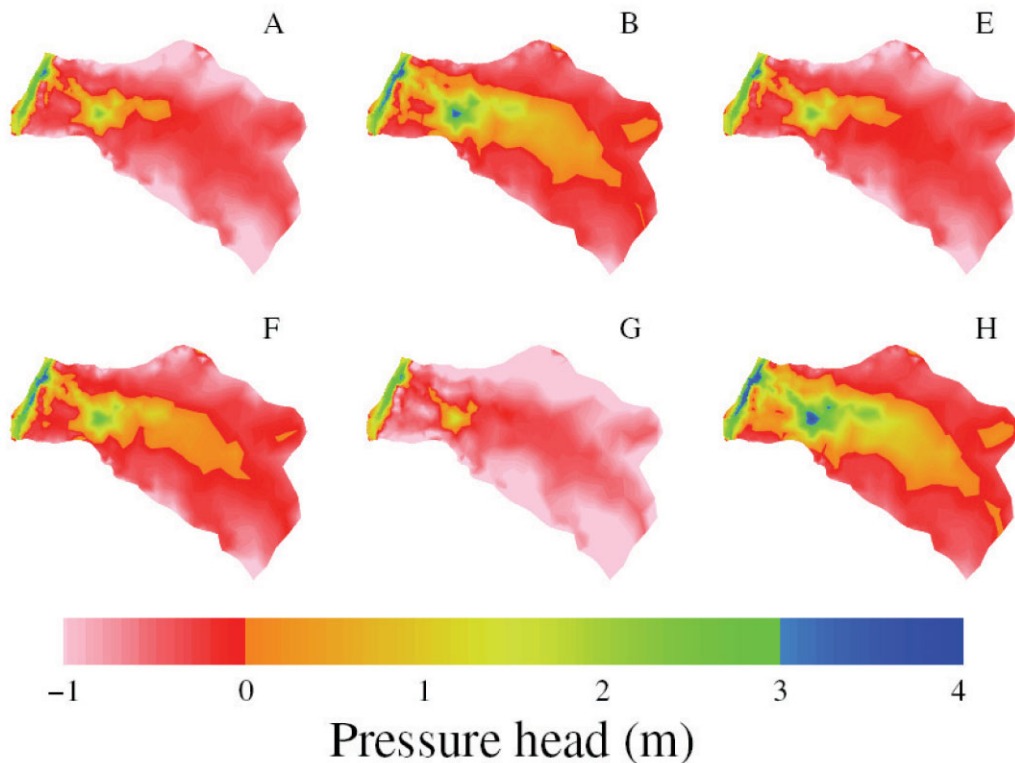§ 2 pm 17 November to 6:30 pm 30 December 1996.

Figure 6. InHM simulated spatially variable C3 pressure head snapshots, at the soil/bedrock interface (see Table II), for times A, B, E, F, G and H in Figure 5.

Figure 6 shows six simulated pressure head snapshots (at the soil/bedrock interface) at times A, B, E, F, G and H in Figure 5. Figure 7 shows six surface water depth snapshots at times A, B, E, F, G and H in Figure 5. Figure 8 shows six snapshots identifying areas of infiltration/exfiltration at times A, B, E, F, G and H in Figure 5. Figure 9 shows one snapshot of the horizontal component of subsurface flow directions (at the soil/bedrock interface) at time H in Figure 5. The dynamics of the InHM simulated hydrologic response for the C3 catchment are predictable on average yet non-intuitive in the details. Perusal of the results in Table III and Figures 5–9 leads to the following general comments.
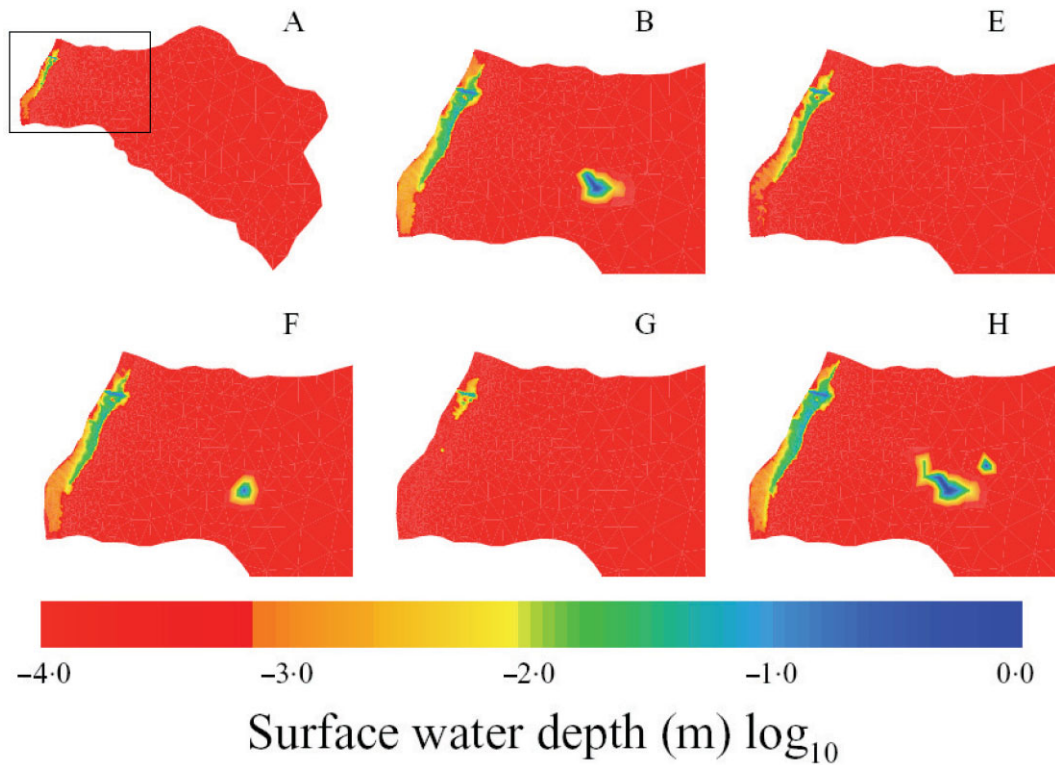
Figure 7. InHM simulated spatially variable C3 surface water depth snapshots for times A, B, E, F, G and H in Figure 5. For the snapshot at time A the entire area of C3 is shown; for snapshots at times B, E, F, G and H only the 0·6 ha area outlined in the snapshot at time A is shown.
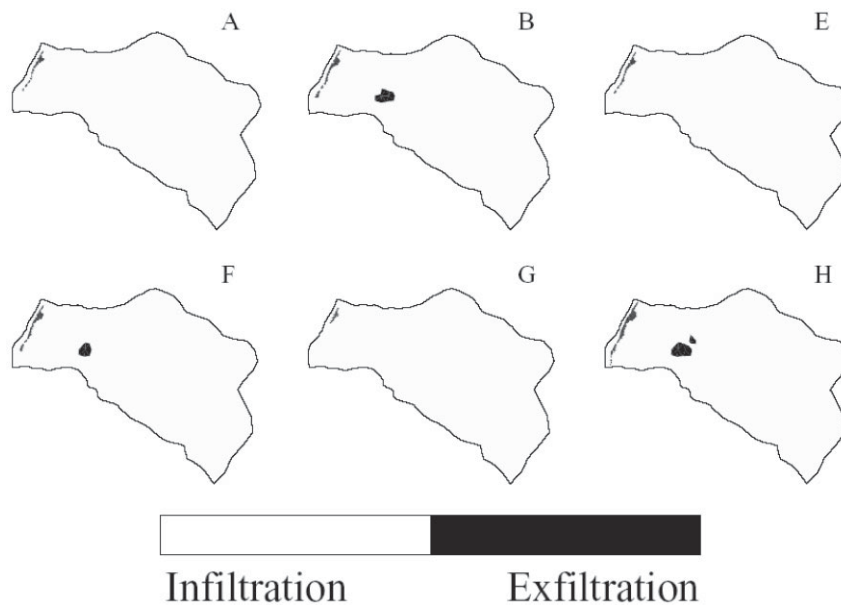

Figure 8. InHM simulated C3 snapshots showing areas of surface infiltration and exfiltration for times A, B, E, F, G and H in Figure 5.
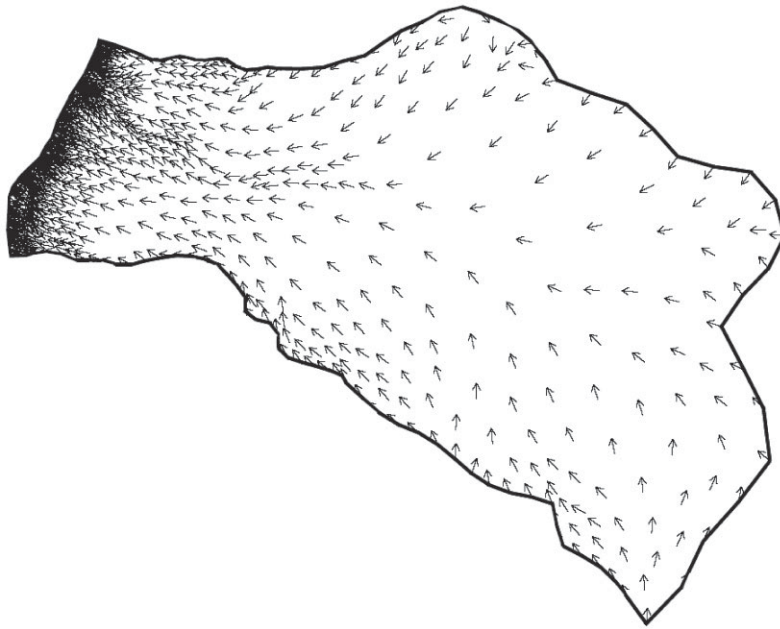
Figure 9. InHM simulated C3 snapshot showing the convergence of subsurface flow for time H in Figure 5.

- Both the timing and magnitude of simulated and observed discharges match well, with runoff events 1–3 better than runoff events 4–6 (see Figure 5).
- Overall model performance is relatively good for the entire 43-day observed record (see Table III).
- Overall model performance ranges from very good to relatively poor for the individual runoff events (Table III).
- Simulated peak discharges are underestimated for five of the six runoff events (see Table III).
- Simulated time to peak discharge is overestimated for four of the six runoff events (see Table III).
- The changes in simulated catchment response during and between storms are significant, while the road remains saturated (see Figure 6).
- Horton overland flow (simulated) occurs along the road for each of the six runoff events (see Figure 7).
- Simulated discharge (from the seepage face) and surface water depths (on the road) are greater for the larger runoff events (e.g. times B and H; see Figure 7).
- Dunne overland flow (simulated) occurs within the topographic depression shown by the closed contour line in Figure 1 and does not contribute to the discharge at the culvert by means of overland flow (see Figures 7 and 8). It is interesting to note that surface saturation was observed at this location during the period shown in Figure 5.
- The road disrupts the up-gradient subsurface flow system (see Figure 8).
- Simulated seepage from subsurface stormflow at the road-cut is the dominant runoff-generation mechanism (see Figure 8).
- The extent of exfiltration from the road-cut varies dynamically, yet persists, throughout the entire simulation period (see Figure 8).
- Subsurface flow (simulated) is convergent into the hollow of the catchment (see Figure 9).

Discussion

Model performance

To the best of our knowledge, there are no established standards (e.g. specific *EF* values) for classifying the performance (e.g. the good, the bad, and the ugly) of comprehensive hydrologic-response models for different applications. It is our opinion, based upon past experience (see table 14 in Loague *et al.* 2005) and given the relatively sparse C3 data set (e.g. (i) limited information on the geometry of the soil/bedrock interface, (ii) no monitoring within the unsaturated

Table IV. Modelling efficiency (*EF*) values for observed C3 discharge values compared to C3 discharge values shifted in magnitude (up/down) and timing (left/right)

	Change in discharge	
EF	**Magnitude (±)** **(percentage (≤))**	**Timing (±)** **(percentage of one day (<))**
1·00	4	2
0·99	5	4
0·98	8	5
0·97	10	6
0·96	12	8
0·95	14	9
0·94	15	10
0·92	18	13
0·90	20	15
0·88	21	17
0·85	24	19
0·83	26	21
0·75	31	27
0·50	44	46
≤0·00	62	100

zone during the simulation period, and (iii) limited characterization of near-surface soil-hydraulic properties), that the performance of InHM in this study was very good.

One major source of poor model performance is less-than-perfect observed data. For example, the relatively poor simulated discharges for runoff events 3 to 5 (i.e. *EF* values of 0·38, −0·29 and 0·49, respectively; see Table III), between the much better estimates for runoff events 1, 2 and 6 (i.e. *EF* values of 0·84, 0·73 and 0·79, respectively; see Table III), may be the result of sediment clogging at the culvert (see Wemple and Jones, 2003). Table IV summarizes the results of considering potential uncertainties in the C3 discharge record. The *EF* values in Table IV were generated from comparisons of the observed discharge record with modified *observed* discharge records (i.e. symmetrical plus and minus scaling in magnitude and shifts in timing). The results in Table IV are not generic and should not be extended beyond the C3 discharge time series example. Inspection of Table 4 leads to three general observations: (i) model performance is relatively insensitive to small changes in magnitude and timing for high *EF* values (e.g. ≥0·97); (ii) differences in magnitude are more important than shifts in timing for smaller changes; and (iii) shifts in timing are more important than shifts in magnitude for larger changes. It is interesting to note that the *EF* value for the entire 43-day simulation period (0·75) corresponds to the *EF* value in Table IV for either a 31 per cent change in magnitude or a 27 per cent change in timing.

Obviously, discharge is not the only observed information that can be in error, subsequently impacting the assessment of model performance. Albeit beyond the scope of this study, uncertainties in rainfall (Burges, 2003), initial conditions (Zehe and Bloschl, 2004) and near-surface soil-hydraulic properties (Loague and VanderKwaak, 2004) are all well known. For example, the rain gauge used in this study is located 400 m below and 2·2 km from the C3 culvert (see Wemple and Jones, 2003).

Convergent flow

The importance of considering convergent flow in the saturated subsurface for the C3 catchment is shown in Figure 9. To further illustrate the importance of 3D effects in process-based hydrologic-response simulations, the C3 BVP was recast as a vertical slice for 2D InHM simulations. Due to differences in how the initial conditions and some boundary conditions were assigned, it was not possible to directly compare the 2D VS2D simulations from Dutton *et al.* (2005) with the 3D InHM simulations in this study. The location of the 2D vertical slice within the C3 catchment is shown in Figure 1. With the exception of dimension, the parameterization of InHM for the 2D BVP is exactly as described herein for the 3D BVP.

The relationship between pressure heads at the 0·5 m (predominantly unsaturated) and 3·0 m (predominantly saturated) for the 3D and 2D InHM simulations at time H in Figure 5 is shown in Figure 10. Inspection of Figure 10
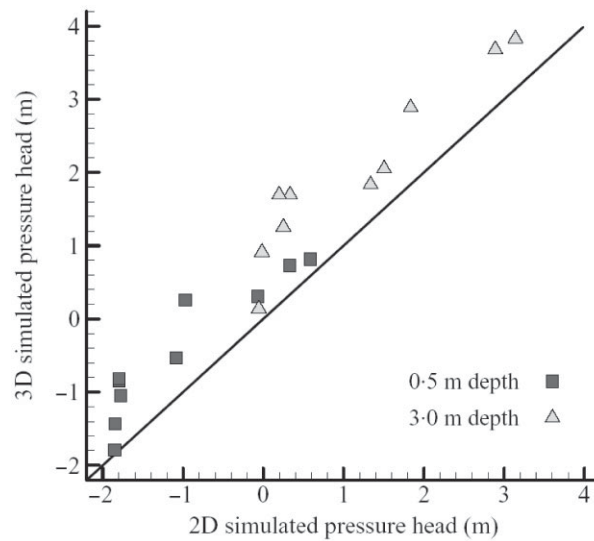
Figure 10. Relationship between unsaturated/saturated pressure heads estimated from 3D and 2D InHM simulations for C3 at time H in Figure 5. The locations of the ten simulated measurement points (0·5 and 3·0 m depths) are shown in Figures 1 and 2.
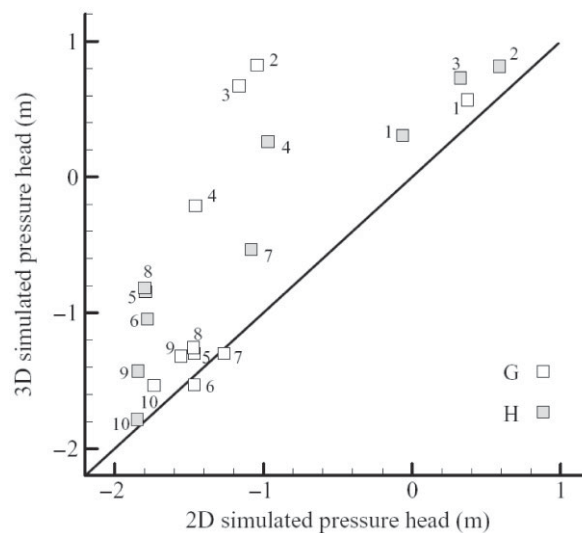

Figure 11. Relationship between pressure heads estimated from 3D and 2D InHM simulations for C3 at times G and H in Figure 5. The ten simulated measurement points (see Figures 1 and 2) are located 0·5 m below the surface.

shows that the 2D simulated pressure heads are lower than the 3D simulated pressure heads. Figures 11 and 12 show the relationships between pressure heads at 0·5 m and at 3·0 m (soil/bedrock interface), respectively, for the 3D and 2D InHM simulations at times G (no rain) and H (rain) in Figure 5. For the upper part of the catchment (i.e. simulated measurement points 5 to 10), inspection of Figures 11 and 12 shows that the 2D simulated pressure heads are closer to 3D simulated pressure heads for the period of no rain compared to the period of rain. For the part of the catchment directly up-gradient of the road (i.e. simulated measurement points 2 to 4), inspection of Figures 11 and 12 shows that the 2D simulated pressure heads are considerably lower than the 3D simulated pressure heads for the period of no rain compared to the period of rain. It is worth noting in Figures 11 and 12, for simulated measurement points 5 to 10, within the rapidly draining upland (i.e. deeper water table), that vertical unsaturated flow dominates, resulting in little difference between the 2D and 3D simulated pressure heads. However, it is also clear from Figure 6 that convergent flow leads to increased saturation near the culvert even between rainfall events. This convergent flow explains the poor performance of the 2D simulation (relative to the 3D simulation) for simulated measurement points 2 to 4,
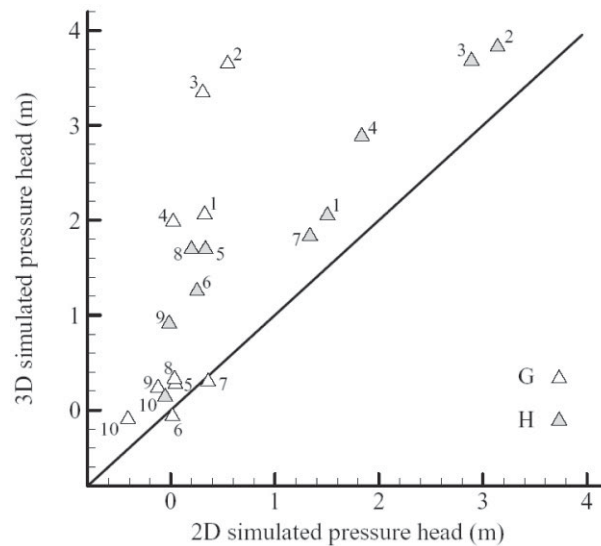
Figure 12. Relationship between pressure heads estimated from 3D and 2D InHM simulations for C3 at times G and H in Figure 5. The ten simulated measurement points (see Figures 1 and 2) are located at 3·0 m below the surface (i.e. the soil/bedrock interface).

particularly between rainfall events (see Figures 11 and 12). Also, the 2D simulation does not maintain the persistent elevated pore-water pressures at the road-cut, shown by the 3D simulation (see simulated measurement points 2 and 3 in Figures 11 and 12).

Slope stability

Dutton *et al.* (2005) reported slope stability estimates for C3 with a 1D infinite-slope model (Selby, 1993) driven by 2D simulations of near-surface hydrologic response for a set of synthetic events. For the infinite-slope model, a slope is estimated to be unstable (subject to failure) when the value of the factor of safety (*FS*) is <1. For this study slope stability estimates were made for the C3 catchment with the infinite-slope model along the long profile (see Figure 1) using pore-water pressures from 3D and 2D (vertical slice) InHM simulations at ten simulated measurement points (see Figures 1 and 2). No geotechnical property information was available for the C3 site. Therefore, the characteristics of the C3 soils were used to make best estimates (Selby, 1993) of the intrinsic cohesion of the soil (1·5 kPa), the root cohesion (5 kPa), the unit weight of the soil (19·6 kNm^{-3}), and the angle of internal friction (35°). The values of the depth from the surface to the shear plane and the slope angle (average along A–A′ in Figure 1) for the C3 BVP are 3 m and 18·3°, respectively.

Table V provides simulated pore-water pressures from the 3D and 2D simulations at time H (see Figure 5) for the simulated monitoring locations (see Figure 2). Inspection of Table V shows, for each of the two hydrologic-response simulation scenarios, that the estimated pore-water pressures are greatest at the culvert (i.e. base of the road-cut) and that the 2D simulated pore-water pressures are lower than 3D simulated pore-water pressures. Figure 13 illustrates the results from the slope stability analyses at time H (see Figure 5) driven by the 3D and 2D simulated pore-water pressures in Table V. Inspection of Figure 13 shows that the lowest *FS* values (i.e. most vulnerable to slope failure), driven by simulated pore-water pressures from the two different hydrologic response simulation scenarios, are at the base of the road-cut and that the *FS* values based upon the 2D simulation are more stable than the *FS* values based upon the 3D simulation. It is worth noting that the drop in the *FS* values at simulated measurement point 7 in Figure 13 can be attributed to the slight topographic depression directly up-gradient.

The infinite slope model used by Dutton *et al.* (2005) and in this study is of only limited value for catchments like C3. For example, the infinite slope model assumes that: (i) failure depth is much less than failure width and length (Iverson, 2000); (ii) the location of the failure plane can be specified *a priori* (Iverson, 2000); (iii) all forces that are not resolvable on planes parallel to the surface are ignored (Iverson, 2000); and (iv) body forces and effective stresses vary only normal to the surface (Iverson and Major, 1986). Clearly these approximations must be improved upon to achieve the same level of process representation for slope stablity as has been described herein for the simulation of

Table V. InHM simulated pore-water pressures for time H in Figure 5 for the locations identified in Figure 2

Simulated monitoring location*	Distance from culvert (m)	Pore-water pressure (kPa)			
		2D simulation		3D simulation	
		0·5 m	3·0 m†	0·5 m	3·0 m†
1	−5·5	−0·6	14·8	3·0	20·1
2	0	5·8	30·8	8·0	37·5
3	1·7	3·2	28·3	7·2	36·1
4	3·8	−9·5	18·0	2·5	28·3
5	9·1	−17·6	3·3	−8·3	16·6
6	28·7	−17·5	2·5	−10·3	12·3
7	50·0	−10·6	13·1	−5·2	18·0
8	95·4	−17·7	1·9	−8·0	16·6
9	124·0	−18·1	−0·2	−14·0	8·9
10	155·4	−18·2	−0·5	−17·5	1·4

* See Figure 1.
† Soil/bedrock contact.
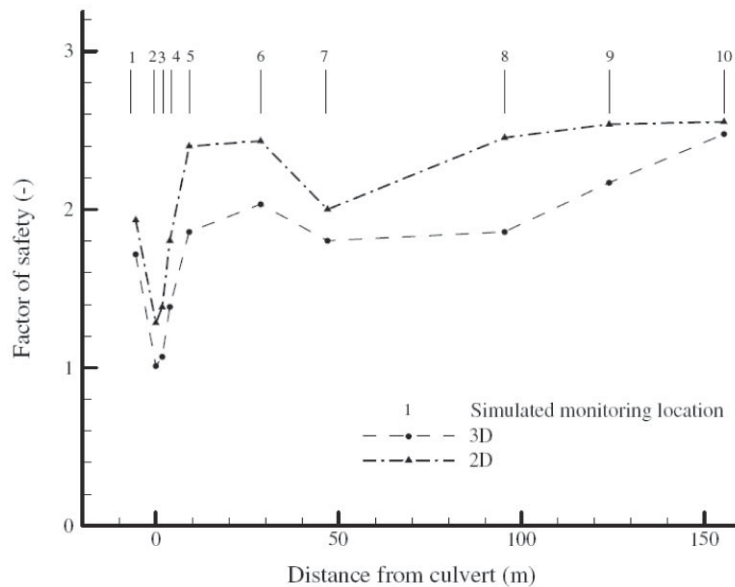
Figure 13. Factor of safety results based upon pore water pressures estimated from 3D and 2D InHM simulations for C3. The ten simulated measurement points (see Figures 1 and 2) are located at the soil/bedrock interface.

hydrologic response. Despite the approximations listed above, the results from the 3D versus 2D hydrologic-response simulations coupled to a simple stability assessment clearly illustrate, in a relative sense, the impact of not considering convergent flow.

Redux versus Dutton *et al.* (2005)

The simulations reported by Dutton *et al.* (2005) cannot be compared directly with the InHM simulations reported herein (i.e. the reason for the 2D InHM simulations in this study). There are four major differences between the hydrologic-response simulations for C3 reported by Dutton *et al.* (2005) and those conducted for this study. The first, and most important, improvement in this study is the consideration of the full 3D problem (e.g. ability to consider convergent lateral inflows). The second difference is the improved characterization of initial conditions, facilitated by

continuous simulation that does not require estimates of antecedent soil-water content for each individual event. The third difference is the improved characterization of process representation (e.g. the exchange of surface/subsurface waters). The fourth difference is how certain boundary conditions can be represented (e.g. unlike the VS2D model used by Dutton *et al.* (2005), InHM does not require an *a priori* location assignment for a potential seepage face). A less major, but significant, difference between the two efforts is that Dutton *et al.* (2005) used a uniform slope, while the best estimate of topography was employed in this study. It should also be noted that the pore pressures used in the slope stability estimates reported by Dutton *et al.* (2005) were from 24 hours after the end of each storm.

Redux limitations

The simulation of hydrologic response for the C3 road problem with InHM, as compared to the effort reported by Dutton *et al.* (2005), provides greater feedback for the understanding/development of process-based concepts. However, the deterministic-conceptual simulations reported herein are not without conceptualization and data-related problems (see Bredehoeft, 2005). For example, little to no information exists for C3 to employ InHM for the following well-known conditions: (i) preferential flow within the near surface (i.e. bypassing via macropores and fractures; Hornberger *et al.*, 1991); (ii) variations in the topography of subsurface units (e.g. the interface between the soil and bedrock layers; Genereux *et al.*, 1993; Freer *et al.*, 2002); (iii) spatial variability in hydrogeologic parameters (Hinton *et al.*, 1993); and (iv) greater spatio-temporal resolution in rainfall intensities.

Summary

The comprehensive hydrologic-response model InHM was employed in this study for 3D simulations of the C3 catchment, clearly demonstrating the importance of convergent subsurface flow and the impact of a forest road. The physics-based 3D simulation illustrates, relative to the spatial evolution of hydrologic response, the development of pressure heads, the distribution of surface water depths, and the extent of infiltration/exfiltration. The spatial and temporal representation of hydrologic response can have important implications for characterizing the geomorphic processes that are associated with forest roads (e.g. seepage erosion, landsliding). Comparisons between 3D and 2D hydrologic-response simulation results and slope stability estimates for C3 events show that both pore-water pressures, and subsequently slope stability, are underestimated without consideration for convergent subsurface flow.

The effort reported here provides a firm quantitative foundation for generalizing the effects of forest roads on near-surface hydrologic response and slope stability at the catchment scale. Additional information, requiring the next generation of field experiments, is needed to fully test InHM.

Acknowledgments

References

Anderson MG, Burt TP. 1977. Automatic monitoring of soil moisture conditions in a hillslope spur and hollow. *Journal of Hydrology* **33**: 27–36.

Anderson MG, Burt TP. 1978. Toward more detailed field monitoring of variable source areas. *Water Resources Research* **14**: 1123–1131.

Anderson MG, Howes S. 1985. Development and application of a combined soil water-slope stability model. *Quarterly Journal of Engineering Geology* **18**: 225–236.

Anderson MG, Kemp MJ, Lloyd DM. 1988. Applications of soil water finite difference models to slope stability problems. In *Proceedings of the Fifth International Symposium on Landslides*, Bonnard C (ed.). A.A. Balkema: Rotterdam; 525–530.

Beven KJ. 1977. Hillslope hydrographs by the finite element method. *Earth Surface Processes* **2**: 13–28.

Beven KJ. 1978. The hydrological response of headwater and sideslope areas. *Hydrological Sciences Bulletin* **23**: 419–437.

Bredehoeft J. 2005. The conceptualization model problem – surprise. *Hydrogeology Journal* **13**: 37–46.

Burges SJ. 2003. Process representation, measurements, data quality, and criteria for parameter estimation of watershed models. In *Calibration of Watershed Models*, Duan Q, Gupta HV, Sorooshian S, Rousseau AN, Turcotte R (eds). American Geophysical Union: Washington, DC; 283–299.

Dhakal AK, Sidle RC, Wu W. 2000. Integrating the hydrologic effects of forest roads into a distributed slope stability model. *EOS, Transactions* **81**: F487.

Dietrich WE, Wilson CJ, Montgomery DR, McKean J, Bauer R. 1992. Channelization thresholds and land surface morphology. *Geology* **20**: 675–679.

Dietrich WE, Wilson CJ, Montgomery DR, McKean J. 1993. Analysis of erosion thresholds, channel networks and landscape morphology using a digital terrain model. *Journal of Geology* **101**: 259–278.

Dietrich WE, Reiss R, Hsu ML, Montgomery DR. 1995. A process-based model for colluvial soil depth and shallow landsliding using digital elevation data. *Hydrological Processes* **9**: 383–400.

Dooge JCI. 1989. Scale problems in hydrology. *Fifth Memorial Chester C. Kisiel Lecture*. University of Arizona, Tucson.

Dunne T. 1990. Hydrology, mechanics and geomorphic implications of erosion by subsurface flow. In *Ground Water Geomorphology: The Role of Subsurface Water in Earth-surface Processes and Landforms*, Higgins CG, Coates DR (eds). Special Paper 252. Geological Society of America: Boulder, CO; 1–28.

Dunne T, Black RG. 1970a. An experimental investigation of runoff production in permeable soils. *Water Resources Research* **6**: 478–490.

Dunne T, Black RG. 1970b. Partial area contributions to storm runoff in a small New England watershed. *Water Resources Research* **6**: 1296–1311.

Dutton AL. 2000. *Process-based simulations of near-surface hydrologic response for a forested upland catchment: The impact of a road*. MS thesis, Stanford University, Stanford, California.

Dutton A, Loague K, Wemple BC. 2005. Simulated effect of a forest road on near-surface hydrologic response and slope stability. *Earth Surface Processes and Landforms* **30**: 325–338.

Engman ET. 1985. Roughness coefficients for routing surface runoff. *Journal of Irrigation and Drainage Engineering* **112**: 39–53.

Fisher JC. 2000. *Simulation of partially saturated-saturated flow in the Caspar Creek E-road groundwater system*. MS thesis, Humboldt State University, Arcata, California.

Freer J, McDonnell JJ, Beven KJ, Peters NE, Burns DA, Hooper RP, Aulenbach BT, Kendall C. 2002. The role of bedrock topography on subsurface storm flow. *Water Resources Research* **38**. DOI: 10.1029/2001WR000872.

Freeze RA. 1971. Three-dimensional transient saturated-unsaturated flow in a groundwater basin. *Water Resources Research* **7**: 347–366.

Freeze RA. 1972a. Role of subsurface flow in generating surface runoff 1. Base flow contributions to channel flow. *Water Resources Research* **8**: 609–624.

Freeze RA. 1972b. Role of subsurface flow in generating surface runoff 2. Upstream source areas. *Water Resources Research* **8**: 1272–1283.

Freeze RA. 1980. A stochastic-conceptual analysis of rainfall-runoff processes on a hillslope. *Water Resources Research* **16**: 391–408.

Freeze RA, Cherry JA. 1979. *Groundwater*. Prentice-Hall: Englewood Cliffs, NJ.

Freeze RA, Harlan RL. 1969. Blueprint for a physically-based digitally simulated, hydrologic response model. *Journal of Hydrology* **9**: 237–258.

Genereux DP, Hemond HF, Mulholland PJ. 1993. Spatial and temporal variability in streamflow generation on the west fork of Walker Branch Watershed. *Journal of Hydrology* **142**: 137–166.

Gilbert GK. 1880. *Report on the Geology of the Henry Mountains*. Government Printing Office: Washington, DC.

Heppner CS, Ran Q, VanderKwaak JE, Loague K. 2006. Adding sediment transport to the Integrated Hydrology Model (InHM): Development and testing. *Advances in Water Resources* **9**: 930–943.

Hinton MJ, Schiff SL, English MC. 1993. Physical properties governing groundwater-flow in a glacial till catchment. *Journal of Hydrology* **142**: 229–249.

Hodge RA, Freeze RA. 1977. Groundwater flow systems and slope stability. *Canadian Geotechnical Journal* **14**: 466–476.

Hornberger GM, Germann PF, Beven KJ. 1991. Throughflow and solute transport in an isolated sloping soil block in a forested catchment. *Journal of Hydrology* **124**: 81–99.

Horton RE. 1945. Erosional development of streams and their drainage basins; hydrophysical approach to quantitative morphology. *Bulletin of the Geological Society of America* **56**: 275–370.

Iverson RM. 2000. Landslide triggering by rain infiltration. *Water Resources Research* **36**: 1897–1910.

Iverson RM, Major JJ. 1986. Groundwater seepage vectors and the potential for hillslope failure and debris flow mobilization. *Water Resources Research* **22**: 1543–1548.

Iverson RM, Reid ME. 1992. Gravity-driven groundwater flow and slope failure potential: 1. Elastic effective stress model. *Water Resources Research* **28**: 925–938.

James LD, Burges SJ. 1982. Selection, calibration and testing of hydrologic models. In *Hydrologic Modeling of Small Watersheds*, Haan CT, Johnson HP, Brakensiek DL (eds). American Society of Agricultural Engineers: St. Joseph, MI; 437–472.

Jones JA, Grant GE. 1996. Peak flow responses to clear-cutting and roads in small and large basins, Western Cascades, Oregon. *Water Resources Research* **32**: 959–974.

Jones JP, Brookfield AE, Sudicky EA. 2004. Quantifying groundwater contributions to streamflow generation: The reliability of tracer-based hydrograph separation techniques. *EOS Transactions AGU* **85**(17) (Joint Assembly Supplment): Abstract H43D-05.

Kirkby MJ, Chorley RJ. 1967. Throughflow, overland flow and erosion. *Bulletin of the International Association of Scientific Hydrology* **12**: 5–21.

Kokkonen T, Koivusalo H, Karvonen T, Croke B, Jakeman A. 2004. Exploring streamflow response to effective rainfall across event magnitude scale. *Hydrological Processes* **18**: 1467–1486.

Lappala EG, Healy RW, Weeks EP. 1993. *Documentation of computer program VS2D to solve the equations of fluid flow in variably saturated porous media*. Water Resources Investigation Report 83-4099, USGS Open File Reports.

Loague K, Green RE. 1991. Statistical and graphical methods for evaluating solute transport models: Overview and application. *Journal of Contaminant Hydrology* **7**: 51–73.

Loague K, VanderKwaak JE. 2002. Simulating hydrologic response for the R-5 catchment: Comparison of two models and the impact of the roads. *Hydrological Processes* **16**: 1015–1032.

Loague K, VanderKwaak JE. 2004. Physics-based hydrologic response simulation: Platinum bridge, 1958 Edsel, or useful tool. *Hydrological Processes* **18**: 2949–2956.

Loague K, Heppner CS, Abrams RH, VanderKwaak JE, Carr AE, Ebel BA. 2005. Further testing of the Integrated Hydrology Model (InHM): Event-based simulations for a small rangeland catchment located near Chickasha, Oklahoma. *Hydrological Processes* **19**: 1373–1398.

Loague K, Heppner CS, Mirus BB, Ebel BA, Ran Q, Carr AE, BeVille SH, VanderKwaak JE. 2006. Physics-based hydrologic-response simulation: Foundation for hydroecology and hydrogeomorphology. *Hydrological Processes* **20**: 1231–1237.

Montgomery DM, Dietrich WE. 1994. A physically based model for the topographic control on shallow landsliding. *Water Resources Research* **30**: 1153–1171.

Montgomery DR, Sullivan K, Greenberg HM. 1998. Regional test of a model for shallow landsliding. *Hydrological Processes* **12**: 943–955.

Montgomery DR, Schmidt KM, Greenberg HM, Dietrich WE. 2000. Forest clearing and regional landsliding. *Geology* **28**: 311–314.

Pack RT, Tarboton DG, Goodwin CC. 1998. The SINMAP approach to terrain mapping. In *Proceedings of the Eighth International Association for Engineering Geology and the Environment*, Moore DP, Hungr O (eds). A.A. Balkema: Rotterdam; 1157–1165.

Pebesma EJ, Switzer P, Loague K. 2005. Error analysis for the evaluation of model performance: Rainfall-runoff time series. *Hydrological Processes* **19**: 1529–1548.

Reid ME, Iverson RM. 1992. Gravity-driven groundwater flow and slope failure potential: 2. Effects of slope morphology, material properties, and hydraulic heterogeneity. *Water Resources Research* **28**: 939–950.

Selby MJ. 1993. *Hillslope Materials and Properties*. Oxford University Press: New York.

Sidle RC, Onda Y. 2004. Hydrogeomorphology: Overview of an emerging science. *Hydrological Processes* **18**: 597–602.

Swanson FJ, Dyrness CT. 1975. Impact of clear-cutting and road construction on soil erosion by landslides in the western Cascade Range, Oregon. *Geology* **3**: 393–396.

Tague C, Band L. 2001. Simulating the impact of road construction and forest harvesting on hydrologic response. *Earth Surface Processes and Landforms* **26**: 135–151.

Thomas RB, Megahan WF. 1998. Peak flow response to clear-cutting and roads in small and large Basins, Western Cascades, Oregon: A second opinion. *Water Resources Research* **34**: 3393–3403.

van Genuchten MTh. 1980. A closed-form equation for predicting the hydraulic conductivity of unsaturated soils. *Soil Science Society of America* **44**: 892–898.

VanderKwaak JE. 1999. *Numerical simulation of flow and chemical transport in integrated surface-subsurface hydrologic systems*. PhD dissertation, University of Waterloo, Waterloo, Ontario, Canada.

VanderKwaak JE, Loague K. 2001. Hydrologic-response simulations for the R-5 catchment with a comprehensive physics-based model. *Water Resources Research* **37**: 999–1013.

Waichler SR, Wemple BC, Wigmosta MS. 2005. Simulation of water balance and forest treatment effects at the H. J. Andrews Experimental Forest. *Hydrological Processes* **19**: 3177–3199.

Wemple BC. 1998. *Investigations of runoff production and sedimentation on forest roads*. PhD dissertation, Oregon State University, Corvallis, OR.

Wemple BC, Jones JA. 2003. Runoff production on forest roads in a steep, mountain catchment. *Water Resources Research* **39**(SWC8): 1220. DOI: 10.1029/2002WR001744.

Wemple BC, Swanson FJ, Jones JA. 2001. Forest roads and geomorphic interactions, Cascade Range, Oregon. *Earth Surface Processes and Landforms* **26**: 191–204.

Wilkinson PL, Anderson MG, Lloyd DM. 2002. An integrated hydrological model for rain-induced landslide prediction. *Earth Surface Processes and Landforms* **27**: 1285–1297.

Wu W, Sidle RC. 1995. A distributed slope stability model for steep forested basins. *Water Resources Research* **31**: 2097–2110.

Zehe E, Bloschl, G. 2004. Predictability of hydrologic response at the plot and catchment scales: Role of initial conditions. *Water Resources Research* **40**: W10202. DOI: 10.1029/2003WR002869.